Active polymer rings: activity-induced collapse and dynamical arrest

Emanuele Locatelli[1,2], Valentino Bianco[3], Paolo Malgaretti[4,5,6]

[1]*Faculty of Physics, University of Vienna, Vienna, Austria*
[2]*Institut für Theoretische Physik, TU Wien, Vienna, Austria*
[3] *Faculty of Chemistry, Chemical Physics Department, Complutense University of Madrid,*
Plaza de las Ciencias, Ciudad Universitaria, Madrid 28040, Spain
[4]*Max Planck Institute for Intelligent Systems, Heisenbergstr. 3, 70569 Stuttgart, Germany*
[5]*IV Institute for Theoretical Physics, University of Stuttgart,*
Pfaffenwaldring 57, 70569 Stuttgart, Germany and
[6]*Helmholtz Institut Erlangen-Nürnberg for Renewable Energy (IEK-11),*
Forschungszentrum Jülich, Fürther Str. 248, 90429, Nürnberg, Germany

We investigate, using numerical simulations, the conformations of isolated active ring polymers. We find that the their behaviour depends crucially on their size: short rings ($N \lesssim 100$) are swelled whereas longer rings ($N \gtrsim 200$) collapse, at sufficiently high activity. By investigating the non-equilibrium process leading to the steady state, we find a universal route driving both outcomes; we highlight the central role of steric interactions, at variance with linear chains, and of topology conservation. We further show that the collapsed rings are arrested by looking at different observables, all underlining the presence of an extremely long time scales at the steady state, associated with the internal dynamics of the collapsed section. Finally, we found that is some circumstances the collapsed state spins about its axis.

Active matter systems, such as synthetic and biological swimmers, show remarkable single particle and collective dynamics that are completely different from their equilibrium counterparts [1]. For example, their active motion leads single active particles to accumulate at walls [2, 3] or at fluid interfaces [4, 5] and to the onset of Motility Induced Phase Separation (MIPS) for dense suspensions [6]. Up to now, the majority of the studies have focuses on "simple" active systems that lack "internal" degrees of freedom, such as colloids. However, recent works on more complex active systems, like active polymers, have shown rich and counter-intuitive dynamics [7–16]. For example, tangentially-active polymers (i.e. polymers for which the active force acts tangentially to their backbone) undergo a coil-to-globule transition upon increasing the activity [13] and show a size-independent diffusion [13, 14].
Such systems are far from being a purely theoretical speculation. Chains of active colloids can be assembled using state-of-the art synthesis techniques[10]; further, experiments with living worms (regarded as tangentially-active polymers) have shown the onset of phase separation [17] akin to active colloids. Moreover, biological filaments such as DNA, RNA, actin and microtubules experience the force of molecular motors [18]. Notably, diverse biological scenarios feature closed structures, i.e. rings or loops, as it happens for DNA and RNA[19–21], extruded loops in chromatin[22, 23], bacterial DNA[24–26], kinetoplast networks[27–29] and actomyosin rings[30, 31]. Finally, topological constraints facilitate packing of long linear macromolecules, a process of capital importance in eukaryotic chromosomes[32–35]. Since the dynamics of ring molecules differs dramatically from that of linear chains [32, 36–40] the question about the dynamics of active rings arises naturally.

In this Letter we characterize, by means of numerical simulations, the conformation and the dynamics of active self-avoiding polymer rings, whose monomers are self-propelled in the direction tangent to the polymer backbone; the rings are unknotted and their topology is preserved at all times.
Our results on active self-avoiding rings show a non-monotonous dependence of the gyration radius on the ring size, in contrast with the monotonous behavior found in both passive rings and active self-avoiding linear chains, highlighting a dramatic change in their dynamics. Moreover we identify the general pathway leading to either inflation (small rings) or collapse (large rings), along with the critical size that separates the basins of attraction of these two steady states.
Since these features are absent for active self-avoiding linear chains clearly they are induced by the topological constraints. We prove this by comparing the dynamics of active self-avoiding rings against that of active ghost-rings (that do not conserve topology). Interestingly, our results show that active ghost-rings swell for all ring sizes, implying that the collapse of active rings is due to activity and collisions among non near-neighboring monomers. Such a feature reminds that of MIPS for Active Brownian Particles (ABP). Finally, focusing on collapsed rings, we find that their internal dynamics shows the hallmarks of dynamical arrest and the onset of a spinning state.

We consider fully flexible bead-spring polymer rings, suspended in an homogeneous fluid in three dimensions. We perform standard Langevin Dynamics simulations neglecting hydrodynamic interactions[41]. The bead diameter σ sets the unit of length, and $m = 1$ sets the unit of mass. The active force $\mathbf{f}^{\text{act}}$ acts with constant magnitude f^{act} along the vector tangent to the polymer backbone [13]; such construction applies to all monomers. We
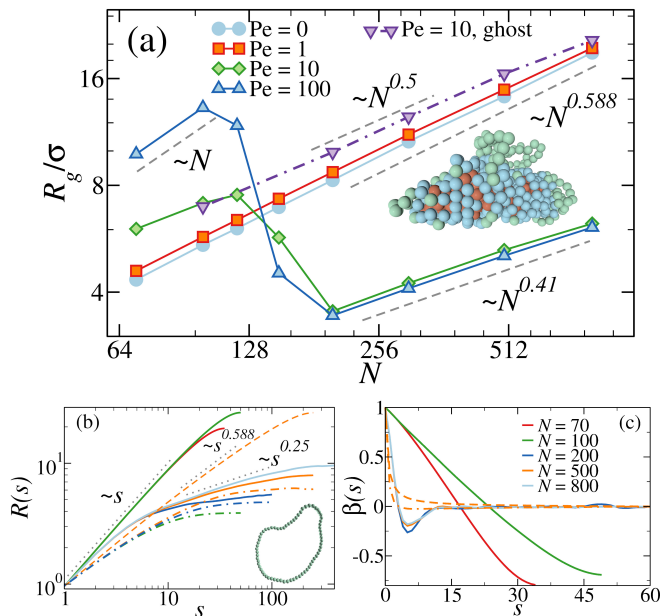
Figure 1. a) Gyration radius as function of N, for active self-avoiding rings (different values of Pe) and active ghost rings (Pe = 10) b) Mean internal distance as function of the distance s along the contour. c) Bond-bond correlation function as function of s. In panel b) and c), full lines refer to active rings at Pe = 100; orange dashed lines refer to the passive case in good solvent for $N = 500$; dash-dotted lines refer to the passive case in bad solvent for $N = 100, 200, 500$. Panels b) and c) share the legend. In panel a) and b) snapshots of short $N = 70$ (inflated) and long $N = 500$ (collapsed) rings, with colors referring to beads: i) in the dangling sections or in the inflated state (green), ii) on the surface of the collapsed structure (blue), iii) in the interior of the collapsed core (red).

quantify the strength of the activity via the Péclet number Pe $\equiv f^{\text{act}}\sigma/(k_B T)$, where $k_B T$ is the thermal energy of the heath bath (being k_B the Boltzmann constant and T the absolute temperature), in which the ring polymer is suspended. Following Ref. [42], we choose to fix $f^{\text{act}}\sigma = 1$ and increase the Péclet number by decreasing the thermal energy of the heath bath.

We employ a modified Kremer-Grest model to avoid crossing events and knots (Sup. Section 1). Hence, we simulate ring polymers of length $70 < N < 800$, at $1 < \text{Pe} < 100$; the data reported are averaged over $250 < M < 2850$ independent configurations.

For tangentially-active linear polymers [13, 14] the average gyration radius $R_g \equiv \sqrt{\langle \sum_{i=1}^{N} (\mathbf{r}_i - \mathbf{r}_{com})^2 / N \rangle}$ – where $\mathbf{r}_i$ and $\mathbf{r}_{com}$ are the positions of the monomer i and center of mass of the polymer, respectively – grows with N with a smaller scaling exponent, compared to the passive case, whose value depends on Pe.

In contrast, for active polymer rings R_g shows a more complex dependence on N (Fig. 1a). In particular, while for Pe $\lesssim 1$ the scaling exponent matches the equilibrium

one $\nu = \nu_{\text{eq}} = 0.588$ for all values of N, for Pe > 1 two distinct regimes emerge, each of which is characterized by a specific scaling of R_g with N. For short rings $N \lesssim 100$, R_g of active rings becomes larger than R_g of passive rings. A power-law fit in this region leads to an exponent, ν_{short}, that depends on Pe: at the largest activity considered (Pe = 100), we find $\nu_{short} \approx 1$, similar to the behaviour of fully rigid rings. Hence, for short rings the activity induces an effective bending rigidity, with a persistence length comparable to the ring's size. Upon increasing the length of the polymers (Fig. 1a), activity induces a structural collapse. In this regime, the scaling exponent is $\nu = \nu_{long} \approx 0.41$ and, for Pe ≥ 10, it is independent on Pe. The small value of ν_{long} indicates that the rings assume a very compact conformation. It is worth noting that the value of ν_{long} is close to, but not exactly the one expected in bad solvent conditions $\nu_{BS} = 0.33$ [43]. Indeed, as shown in the snapshot in Fig. 1a, the collapsed structure is quite complex, being composed of a compact self-wrapped core and few *dangling sections* fluttering on its surface. These dangling sections, absent in the case of ring polymers in bad solvents [44], are responsible for the larger value of ν_{long} as compared to ν_{BS} (Sup. Section 6). Moreover, upon increasing Pe, the transition between inflated and collapsed rings becomes progressively sharper. We elucidate the role of self-avoidance in this phenomenon by simulating active ghost rings that, by contrast, maintain their passive scaling $N^{0.5}$ for all values of N investigated (see the violet curve in Fig. 1a); further, activity swells the rings, without further altering their configurational properties (Sup.Fig. 7).

To understand the physical origin of the scaling regimes observed, we analyze the conformations attained by long and short active rings. Accordingly, we compute, in the steady state, the root mean square distance among monomers that are s-th neighbors along the backbone $R(s) \equiv \sqrt{\langle (\mathbf{r}_{s+s_0} - \mathbf{r}_{s_0})^2 \rangle}$ where s_0 is the starting bead.

Fig. 1b shows that for short rings $R(s)$ displays a single power law trend $R(s) \sim s$ whose exponent is compatible with the one estimated from the scaling of the gyration radius in Fig. 1a. The *single* power law fitting $R(s)$ up to $s \simeq N/2$ implies the self-similarity of active rings. For reference, we report $R_{eq}(s)$ for fully-flexible passive rings in good solvents, for which $R_{eq}(s) \simeq s^{0.588}$ [44] (orange dashed lines in Fig. 1b). In contrast, longer active rings show a richer behaviour for $R(s)$. Indeed, for $s \lesssim 10$, $R(s)$ shows a universal power law $R(s) \sim s$ whose prefactor does not depend on N (all curves collapse on a master curve in Fig. 1b). Then, for $s \gtrsim 10$, the scaling of $R(s)$ is size-dependent and, for intermediate values of s, is fitted by $R(s) \simeq s^{0.25}$. This change is the signature of the collapsed structure: monomers very far away along the backbone end up being very close in real space. This behaviour is qualitatively similar to that observed
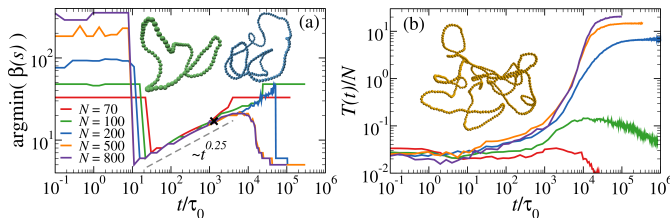
Figure 2. Route to the steady state: (a) position of the minimum of the bond correlation (b) Tangleness $T(t)/N$ as a function of time, normalized by τ_0, for rings of different length at Pe =100. The black symbol in panel (a) marks the time at which the snapshots shown are taken. Snapshots: $N = 100$ green, $N = 200$ blue, $N = 500$ orange.

for passive rings in bad solvents (dashed-dotted curves in Fig. 1b).

In order to characterize the local arrangement of monomers in the inflated/collapsed states we measure the bond-bond spatial correlation function $\beta(s) \equiv \langle \mathbf{b}_{s+s_0} \cdot \mathbf{b}_{s_0} \rangle$, where $\mathbf{b}_i \equiv \mathbf{r}_{i+1} - \mathbf{r}_i$.

As shown in Fig. 1c, short active rings $N = 70, 100$ develop a strong anti-correlation over the scale of the whole polymer, akin of rigid passive rings. In contrast, for long active rings, the bond-bond correlation function shows a very fast decay at small contour separations, followed by an anti-correlation region that eventually fades to a complete decorrelation. In the collapsed state, part of the chain wraps on itself (Sup.Fig. 11) and such wrappings are characterized by a "pitch" of ~ 5 beads which is, roughly, at the same contour distance $s \simeq 5$ for all N and Pe investigated. These behaviors are in contrast to those observed for passive rings in both good (dashed orange curve) and bad solvents (dotted orange curve) that display no minimum at short contour separations.

Next we investigate the pathway from a passive, equilibrated ring configuration to the inflated/collapsed steady state, by considering the time evolution of the bond correlation function $\beta(t)$ and the square average contour distance between pairs of beads that are close in space $T(t) = \langle \left((j - j_1)^2 + \ldots + (j - j_m)^2 \right) / m \rangle$ that measures the "tangleness" of a polymer chain (see Sup. Eq.(7)). In particular, Fig. 1c shows that $\beta(s)$ is characterized by a minimum, either at small s or $s = N/2$. We follow the evolution in time of the contour length at which such minimum appears, $\mathrm{argmin}(\beta(s))$, as it marks the characteristic size of the local structures that form along the polymer backbone (Fig. 2a). For passive rings, the minimum is at $\sim N/2$ for all times. This coincides with the value obtained for active rings at early times ($t \leq 10\tau_0$); during such time frame, comparable to the diffusion time $\tau_0 = \sigma^2/D$ of a monomer over its size, activity has not yet affected the conformation of the ring. At intermediate times, $t \simeq 10\tau_0 - 1000\tau_0$ (Fig. 2), small "loops" appear, highlighted by a drop of the minimum of the

bond correlation to $s \simeq 5$, roughly constant for all N. Their sharp onset takes place at earlier times upon increasing the polymer size ($\sim 20\tau_0$ for $N = 70$, $\sim 10\tau_0$ for $N = 500$) and it is weakly dependent on Pe, for Pe $\gtrsim 10$. The size of the loops grows up to a characteristic size s, reached in $t \in [\sim 10^3\tau_0 : 10^4\tau_0]$, with a growth rate $\propto (t/\tau_0)^{1/4}$ essentially independent of N and Pe (Sup.Fig. 9b), hence setting an universal route towards the steady state. This universal growth $\propto t^{1/4}$ reminds of the coarsening of $2D$ ABPs undergoing MIPS [45, 46]. Snapshots of rings taken during this stage are reported in Fig. 2; loops are clearly visible in all cases irrespective of N. At later times, the dynamics is no more universal and the size of the ring matters.

For $N \lesssim 100$, loops of size $s \simeq 20$ are relatively close to their equilibrium value $N/2$. When two loops meet they merge giving raise to a larger loop (see the jumps in $\beta(s)$ in Fig. 2.a for $N = 70, 100$). At variance, for $N > 200$ (Sup. Video 1) when two loops of size $s \simeq 20$ get closer they can thread one into the other, triggering a cascade of collisions that drives sections of the backbone to tangle, inducing the collapse of the entire chain. After such a catastrophic event, the rest of the ring is progressively recruited in the main tangle (see Sup. Video 1). Such a scenario is also supported by the tangleness $T(t)$. Indeed, we observe the tangleness per size $T(t)/N$, at very short times, i.e. when activity has not yet affected the ring, has a characteristic value, dependent on the chosen cut-off radius r_c (defining spatial neighbours) and independent on N. Afterwards, the behaviour of $T(t)/N$ depends on the final steady state. For short, inflating rings, the tangleness shows a shallow maximum and then decreases towards a small constant value. In contrast, for long collapsing rings, $T(t)/N$ monotonically increases toward a large constant value. This increment develops on roughly the same timescales as the growth of $\mathrm{argmin}(\beta(s))$ but, further, shows two regimes, characterised by a mild increase first and a steeper slope later on. The increase of $T(t)$ can be thus directly connected with an increase of the steric interactions and with collisions. $T(t)$ and $\mathrm{argmin}(\beta)$ appear complementary to each other: the tangleness better captures the "two-steps" collapse, while $\mathrm{argmin}(\beta(s))$ better highlights the universality of this route. The polymers conformations along the pathway can be further characterised with the torsional order parameter (Sup.Fig. 11). We remark that the collapsed state is, in its origin, akin to MIPS [47], as both are initiated by collisions and maintained by self-avoidance. This confirms the result reported for ghost rings: without self-avoidance, tangles can't form and the rings are effectively composed by non-interacting loops (Sup.Fig. 5). The described pathway is common for sufficiently high Pe, while for Pe $\lesssim 5$ sufficiently long rings may end up in a collapsed state following a much smoother route (Sup.Fig. 10).

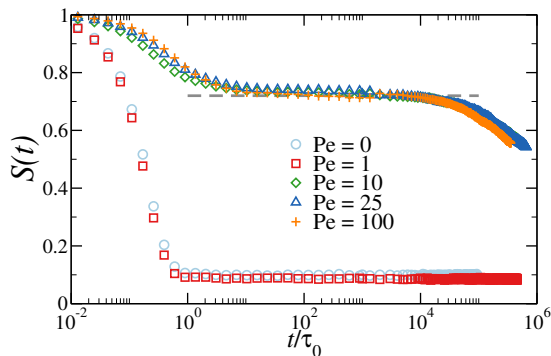After the collapse, monomers in the tangle find them-

Figure 3. Fraction of survived neighbours as function of time; data refer to rings of size $N = 500$ and several Pe at the steady state. The gray dashed line is a guide for the eye, highlighting the intermediate plateau.
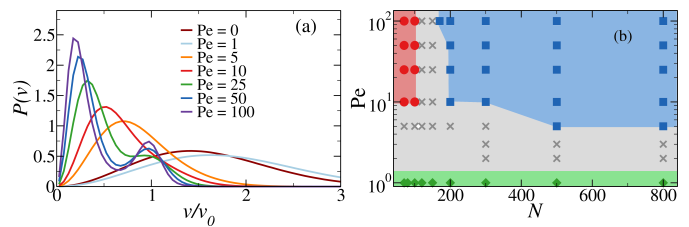

Figure 4. a) Monomer velocity distributions at the steady state for fixed $N = 500$, several Pe. b) Dynamic phase diagram for active rings. Symbols refer to state points sampled by means of numerical simulations: collapsed rings are reported as blue squares, inflated rings as red circles, passive-like rings as green diamonds, system showing a more complex behaviour as grey crosses.

selves in a complex and tight structure whose dynamics, in the steady state, is arrested. This can be verified by computing the surviving fraction of neighbours $S(t)$, defined as the fraction of monomer's neighbours within a radius r_c (excluding the first-neighbors along the backbone), chosen at any arbitrary time t_0 during the steady state, that are still neighbours of the same monomer at $t > t_0$. We fix the neighbouring cut-off $r_c = 1.2\sigma$. Since $S(t)$ provides a measure of the permanence of the collapsed configurations we expect $S(t) \sim 1$ for a completely frozen system, otherwise $S(t)$ decays to a small non-vanishing value after a characteristic time. Fig. 3 shows $S(t)$ for $N = 500$ and increasing activity (Pe$\in [0 : 100]$). For Pe $<= 1$ rings are not collapsed and $S(t)$ displays a fast decay and plateaus to a small value akin of passive rings [48]. As soon as the rings collapse (Pe ≥ 10) $S(t)$ shows a strikingly different behaviour. First, at short times ($t <= \tau_0$), $S(t)$ decays mildly due to the highly mobile dangling sections. This decay occurs on time scale comparable to that of passive rings, but with reduced magnitude. The initial decay is followed by a plateau that lasts several decades and whose time-span is slightly dependent on N (Sup. Fig. 16). Afterwards, a second decay is observed, which possibly plateaus at later times (outside the time frame of the simulations). This double decay can be found also in the intermediate scattering function and in the time correlation of the characteristic vectors of the ring (Sup.Fig. 18-21). Overall, for every observable considered, the first decay is due to the the contribution of the dangling sections, whereas the second, much slower, is related to the complete rearrangement of the beads neighbouring environment within a length scale of the order of σ.

A hallmark of an arrested dynamics appears also in the distribution of the instantaneous velocities of the monomers at steady state (Fig. 4a). As expected, at equilibrium (Pe $= 0$) the distribution is Maxwell-Boltzmann. Interestingly, for Pe $\lesssim 1$ the distribution

is again Maxwell-Boltzmann but with an effective temperature $T_{eff} \simeq 1.3 \ k_B T^\star$, "heating up" the rings. At sufficiently high Pe, the distributions exhibit two peaks, at $v << v_0$ and $v \sim v_0$ rispectively. In Fig. 4a , the peak at small velocities is given by the monomers trapped in the collapsed section (Sup.Fig. 22), whereas the peak at $\nu/\nu_0 \sim 1$ is due to monomers in the dangling sections. Such velocity distributions remind those observed in MIPS, where active particles inside the dense phase-separated region experience a reduced mobility with respect to their counterparts in the gas phase [49–51]. In particular, comparing Fig. 4 with Figs. 1,3 we note that the velocity distribution varies continuously upon increasing Pe, whereas nor the R_g neither $S(t)$ are sensitive to such a change. This implies that the configuration of the polymers, and hence the onset of MIPS-like transition, is robust to changes in the velocity distribution provided that both Pe and N are large enough.

We collect our data into a phase diagram shown in Fig. 4b, where four regions can be identified according to the scaling of R_g with N. At small Pe, active rings retain their equilibrium scaling for all values of N. For Pe $\gtrsim 10$, the scaling of R_g with N depends on the active ring size: smaller active rings ($N \lesssim 100$) swell ($R_g \propto N$), whereas larger active rings ($N \gtrsim 200$) display arrested, collapsed configurations with dangling sections. The transition between these two "phases" occurs via a transition region, of finite extent, in which the dependence of R_g on N is more complex (see Fig. 1) and can be either jumping in between fairly compact and fairly open conformation (typical for $100 < N < 200$) or quasi-collapsed but not arrested conformations (typical for Pe < 5 and $N > 300$)(Sup. Videos 3 and 4). Finally, the supplemental video 1 and 2 show a rotating motion and self-propulsion of the collapsed state, due to an active torque and a non-zero net active force on the centre of mass, respectively (Sup.Fig. 23 and 20a).

In summary, we have presented the effects of tangential activity on the conformation of fully flexible self-avoiding active ring polymers. We have shown that, upon increas-

ing the activity, there is a conformational transition between short rings ($N \lesssim 100$) that swell and assume a disk-like shape, and long rings ($N \gtrsim 200$) that exhibit a structural collapse. The non-equilibrium evolution towards the steady state follows a general route featuring loop formation growing in size up to a characteristic size ~ 20. Then, for sufficiently long rings, the collapse is triggered by clashes between monomers belonging to non-neighbouring loops. Finally, the extremely slow structural relaxation of different observables, indicates that the collapsed rings represent a unique example of arrested macromolecule. These features are typical of tangentially-active ring polymers and may disappear in case of isotropic [52] or scalar [53] activity. Neglecting hydrodynamics has allowed us to robustly investigate rings of large size for long time scales. Nevertheless, hydrodynamic interactions will be crucial to investigate the dynamics and the stability of the open conformations at small values of N[54]. Granted the phenomenology observed in this paper is robust, active rings may be exploited to wrap, protect and deliver drugs. Further, topology-based materials have been already proposed[55], for which activity may change the macroscopic properties, as happens for biopolymer networks[56]. Possibly, the most exciting application concerns the modeling of self-propelled filaments in gliding assays[57] and of biophysical systems, exploring the effect of activity in chromatin[58–60], in bacterial DNA and in the cytoskeleton[61–63], where actomyosing ring may play a key role in cell division[64], or in purified protein networks[56, 65, 66].

---

[1] C. Bechinger, R. Di Leonardo, H. Löwen, C. Reichhardt, G. Volpe, and G. Volpe, Rev. Mod. Phys. **88**, 045006 (2016).

[2] A. P. Berke, L. Turner, H. C. Berg, and E. Lauga, Phys. Rev. Lett. **101**, 038102 (2008).

[3] J. Elgeti and G. Gompper, EPL (Europhysics Letters) **101**, 48003 (2013).

[4] R. Di Leonardo, D. Dell'Arciprete, L. Angelani, and V. Iebba, Phys. Rev. Lett. **106**, 038101 (2011).

[5] P. Malgaretti, M. N. Popescu, and S. Dietrich, Soft Matter **14**, 1375 (2018).

[6] M. E. Cates and J. Tailleur, Annual Review of Condensed Matter Physics **6**, 219 (2015).

[7] A. Kaiser, S. Babel, B. Ten Hagen, C. Von Ferber, and H. Löwen, Journal of Chemical Physics **142** (2015), 10.1063/1.4916134.

[8] T. Eisenstecken, G. Gompper, and R. G. Winkler, Polymers **8**, 37 (2016).

[9] R. E. Isele-Holder, J. Elgeti, and G. Gompper, Soft Matter **11**, 7181 (2015).

[10] J. Yan, M. Han, J. Zhang, C. Xu, E. Luijten, and S. Granick, Nature Materials **15**, 1095 (2016).

[11] H. R. Vutukuri, B. Bet, R. Van Roij, M. Dijkstra, and W. T. Huck, Scientific Reports **7**, 1 (2017).

[12] S. Gonzalez and R. Soto, New Journal of Physics **20** (2018), 10.1088/1367-2630/aabe3c.

[13] V. Bianco, E. Locatelli, and P. Malgaretti, Phys. Rev. Lett. **121**, 217802 (2018).

[14] S. K. Anand and S. P. Singh, Phys. Rev. E **98**, 042501 (2018).

[15] M. Foglino, E. Locatelli, C. Brackley, D. Michieletto, C. Likos, and D. Marenduzzo, Soft matter **15**, 5995 (2019).

[16] S. Das and A. Cacciuto, Physical review letters **123**, 087802 (2019).

[17] A. Deblais, A. Maggs, D. Bonn, and S. Woutersen, Physical Review Letters **124**, 208006 (2020).

[18] B. Alberts, A. Johnson, J. Lewis, M. Raff, K. Roberts, and P. Walter, *Molecular Biology of the Cell* (Garland Science, Oxford, 2007).

[19] R. Schleif, Annual review of biochemistry **61**, 199 (1992).

[20] J.-F. Allemand, S. Cocco, N. Douarche, and G. Lia, The European Physical Journal E **19**, 293 (2006).

[21] S. Semsey, K. Virnik, and S. Adhya, Trends in biochemical sciences **30**, 334 (2005).

[22] A. Goloborodko, J. F. Marko, and L. A. Mirny, Biophysical journal **110**, 2162 (2016).

[23] W. Schwarzer, N. Abdennur, A. Goloborodko, A. Pekowska, G. Fudenberg, Y. Loe-Mie, N. A. Fonseca, W. Huber, C. H. Haering, L. Mirny, *et al.*, Nature **551**, 51 (2017).

[24] A. Worcel and E. Burgi, Journal of molecular biology **71**, 127 (1972).

[25] L. Postow, C. D. Hardy, J. Arsuaga, and N. R. Cozzarelli, Genes & development **18**, 1766 (2004).

[26] X. Wang, P. M. Llopis, and D. Z. Rudner, Nature Reviews Genetics **14**, 191 (2013).

[27] P. Borst and J. H. Hoeijmakers, Plasmid **2**, 20 (1979).

[28] Y. Diao, V. Rodriguez, M. Klingbeil, and J. Arsuaga, Plos one **10**, e0130998 (2015).

[29] A. R. Klotz, B. W. Soh, and P. S. Doyle, Proceedings of the National Academy of Sciences **117**, 121 (2020).

[30] I. M. Sehring, P. Recho, E. Denker, M. Kourakis, B. Mathiesen, E. Hannezo, B. Dong, and D. Jiang, Elife **4**, e09206 (2015).

[31] S. P. Pearce, M. Heil, O. E. Jensen, G. W. Jones, and A. Prokop, Bulletin of Mathematical Biology **80**, 3002 (2018).

[32] A. Grosberg, Y. Rabin, S. Havlin, and A. Neer, EPL (Europhysics Letters) **23**, 373 (1993).

[33] A. Rosa and R. Everaers, PLoS Comput Biol **4**, e1000153 (2008).

[34] A. Rosa, Biochemical Society Transactions **41**, 612 (2013).

[35] J. D. Halverson, J. Smrek, K. Kremer, and A. Y. Grosberg, Reports on Progress in Physics **77**, 022601 (2014).

[36] M. Frank-Kamenetskii, A. Lukashin, and A. Vologodskii, Nature **258**, 398 (1975).

[37] M. Cates and J. Deutsch, Journal de physique **47**, 2121 (1986).

[38] M. Rubinstein, Physical review letters **57**, 3023 (1986).

[39] A. Y. Grosberg, S. K. Nechaev, and E. I. Shakhnovich, Journal de physique **49**, 2095 (1988).

[40] C. Micheletti, D. Marenduzzo, and E. Orlandini, Physics Reports **504**, 1 (2011).

[41] Such an approximation is made in the spirit of "dry active matter" that has identified the onset of activity-induced phase separation (known as MIPS), later observed also in experiments (hence where hydrodynamic coupling is present). Similarly, we expect that our results will qualitatively persist even in the presence of hydrodynamic coupling .

[42] J. Stenhammar, D. Marenduzzo, R. J. Allen, and M. E. Cates, Soft Matter **10**, 1489 (2014).

[43] M. Doi, *Introduction to polymer physics* (Clarendon Press, Oxford science publications, 1996).

[44] M. Rubinstein, R. H. Colby, *et al.*, *Polymer physics*, Vol. 23 (Oxford university press New York, 2003).

[45] J. Stenhammar, A. Tiribocchi, R. J. Allen, D. Marenduzzo, and M. E. Cates, Phys. Rev. Lett. **111**, 145702 (2013).

[46] A. Patch, D. Yllanes, and M. C. Marchetti, Phys. Rev. E **95**, 012601 (2017).

[47] M. E. Cates and J. Tailleur, Annu. Rev. Condens. Matter Phys. **6**, 219 (2015).

[48] We remark that such value is not strictly zero, as relatively close monomers can randomly get in and out of the threshold range chosen ($r_c =$1.2 σ.).

[49] R. Sánchez and P. Díaz-Leyva, Physica A: Statistical Mechanics and its Applications **499**, 11 (2018).

[50] S. Mandal, B. Liebchen, and H. Löwen, Phys. Rev. Lett. **123**, 228001 (2019).

[51] L. Caprini and U. Marini Bettolo Marconi, ArXiV **arXiv:2009.07234** (2020).

[52] S. M. Mousavi, G. Gompper, and R. G. Winkler, Journal of Chemical Physics **150** (2019), 10.1063/1.5082723.

[53] J. Smrek, I. Chubak, C. N. Likos, and K. Kremer, Nature communications **11** (2020).

[54] M. Liebetreu and C. N. Likos, Communications Materials **1**, 1 (2020).

[55] B. A. Krajina, A. Zhu, S. C. Heilshorn, and A. J. Spakowitz, Physical review letters **121**, 148001 (2018).

[56] G. H. Koenderink, Z. Dogic, F. Nakamura, P. M. Bendix, F. C. MacKintosh, J. H. Hartwig, T. P. Stossel, and D. A. Weitz, Proceedings of the National Academy of Sciences **106**, 15192 (2009).

[57] L. Liu, E. Tüzel, and J. L. Ross, Journal of Physics: Condensed Matter **23**, 374104 (2011).

[58] T. Terakawa, S. Bisht, J. M. Eeftens, C. Dekker, C. H. Haering, and E. C. Greene, Science **358**, 672 (2017).

[59] D. Saintillan, M. J. Shelley, and A. Zidovska, Proceedings of the National Academy of Sciences **115**, 11442 (2018).

[60] K. A. Haushalter and J. T. Kadonaga, Nature Reviews Molecular Cell Biology **4**, 613 (2003).

[61] G. Danuser, J. Allard, and A. Mogilner, Annual review of cell and developmental biology **29**, 501 (2013).

[62] M. Murrell, P. W. Oakes, M. Lenz, and M. L. Gardel, Nature reviews Molecular cell biology **16**, 486 (2015).

[63] D. A. Fletcher and R. D. Mullins, Nature **463**, 485 (2010).

[64] T. Litschel, C. F. Kelley, D. Holz, M. A. Koudehi, S. K. Vogel, L. Burbaum, N. Mizuno, D. Vavylonis, and P. Schwille, BioRxiv (2020).

[65] S. Stam, S. L. Freedman, S. Banerjee, K. L. Weirich, A. R. Dinner, and M. L. Gardel, Proceedings of the National Academy of Sciences **114**, E10037 (2017).

[66] F. Burla, Y. Mulla, B. E. Vos, A. Aufderhorst-Roberts, and G. H. Koenderink, Nature Reviews Physics **1**, 249 (2019).

[67] S. Plimpton, J Comp Phys **117**, 1 (1995).

[68] K. Kremer and G. S. Grest, J. Chem. Phys. **92**, 5057 (1990).

[69] R. Chelakkot, R. G. Winkler, and G. Gompper, Physical review letters **109**, 178101 (2012).

[70] L. Tubiana, G. Polles, E. Orlandini, and C. Micheletti, EPJ E **41**, 72 (2018).

[71] P.-G. de Gennes, *Scaling Concepts in Polymer Chemistry* (University Press, Ithaca, NY, 1979).

[72] C. Kurzthaler, S. Leitmann, and T. Franosch, Scientific reports **6**, 36702 (2016).

Supplemental Material

Emanuele Locatelli[1,2], Valentino Bianco[3], Paolo Malgaretti[4,5,6]
[1] *Faculty of Physics, University of Vienna, Vienna, Austria*
[2] *Institut für Theoretische Physik, TU Wien, Vienna, Austria*
[3] *Faculty of Chemistry, Chemical Physics Department, Complutense University of Madrid,*
Plaza de las Ciencias, Ciudad Universitaria, Madrid 28040, Spain
[4] *Max Planck Institute for Intelligent Systems, Heisenbergstr. 3, 70569 Stuttgart, Germany*
[5] *IV Institute for Theoretical Physics, University of Stuttgart,*
Pfaffenwaldring 57, 70569 Stuttgart, Germany and
[6] *Helmholtz Institut Erlangen-Nürnberg for Renewable Energy (IEK-11),*
Forschungszentrum Jülich, Fürther Str. 248, 90429, Nürnberg, Germany

MODEL

We model ring polymers as bead-spring chains in three dimensions; the bead diameter, σ, sets the unit of length, and m sets the unit of mass. We perform standard Langevin Dynamics simulations using a custom modified version of LAMMPS[67], neglecting at this stage hydrodynamic interactions; we set the friction coefficient $\gamma = 1$ and the elementary timestep $\Delta t = 10^{-3}$. The requirement of the topology conservation, i.e. maintaining the rings unknotted, requires special care in modeling the activity and in choosing the interaction potentials. First, each monomer is self-propelled by a force $\mathbf{f}^{\text{act}}$, with constant magnitude f^{act}. The direction of $\mathbf{f}_i^{\text{act}}$ is always parallel to $\mathbf{r}_{i+1,i-1} \equiv \mathbf{r}_{i+1} - \mathbf{r}_{i-1}$, i.e the vector connecting the first neighbours of monomer i along the polymer backbone; such construction applies to all monomers. As standard in active systems, we quantify the activity of each monomer by the Péclet number Pe

$$\text{Pe} \equiv \frac{f^{\text{act}}\sigma}{k_B T} \tag{1}$$

where $k_B T$ is the thermal energy of the heath bath, in which the polymer is suspended. In the spirit of [42], we choose to fix $f^{\text{act}} = 1$ and we change the Péclet number by decreasing the thermal energy. This is equivalent to set a reference temperature $T^\star$, such that $k_B T^\star = 1$.

This simulation strategy allows us to avoid the introduction of huge forces in the system and to use a reasonably small timestep. Further, in order to avoid crossing events we choose to employ a modified Kremer-Grest model.
The original Kremer-Grest model[68] preserves the topology in absence of activity and is widely used as generic force field for self-avoiding polymers. However, as already mentioned, in presence of activity long rings tend to collapse; we find that this state is particularly prone to knot formation as the backbone is rather stressed and bonds tend to stretch. The Kremer-Grest model, employing a standard FENE potential, allows for considerable stretching, as the maximum distance is $R_{max} = 1.5\sigma$ whereas the typical distance (typical bond length) is $b \simeq 0.97\ \sigma$. In principle, crossings are possible in absence of activity but, in practice, in equilibrium the energy barrier is so high ($\sim 70\ k_B T$) that crossings are negligible. This is, clearly, not true in the collapsed state considered, because of the self-avoidance as well as of the active forces. In principle, the use of a much smaller time-step (e.g. $\Delta t \leq 10^{-6}$) would solve the problem at the cost of making the long time dynamics inaccessible. In order to avoid crossing events at the chosen time step $\Delta t = 10^{-3}$, we choose to employ a WCA-like potential between any pair of monomers

$$V_{mm}(r) = \begin{cases} 4\epsilon \left[\left(\frac{\sigma}{r}\right)^{44} - \left(\frac{\sigma}{r}\right)^{22} \right] + \epsilon; & \text{for } r < 2^{1/22}\,\sigma, \\ 0; & \text{for } r \geq 2^{1/22}\,\sigma, \end{cases} \tag{2}$$

with $\epsilon =1$; further, neighbouring beads along the backbone are bonded by a FENE potential

$$V_{\text{FENE}}(r) = \begin{cases} -150\epsilon \left(\frac{R_{\max}}{\sigma}\right)^2 \ln \left[1 - \left(\frac{r}{R_{\max}}\right)^2 \right]; & \text{for } r \leq R_{\max}, \\ \infty; & \text{for } r > R_{\max}, \end{cases} \tag{3}$$

with $R_{\max} =1.05$. Such potential is much steeper and imposes a much smaller range of fluctuations than the standard Kremer-Grest model; the bonds never stretch more than 1-2 % of their typical value $b \simeq 0.96\ \sigma$ (see Fig. 6). Having a typical bond length as similar to the original as possible was the rationale behind the choice of the parameters for

this force field. We point out that such hard and tight bonds are necessary only for very long rings; short rings do not collapse and standard Kremer-Grest potentials with $\epsilon = 10$ is sufficient to preserve the topology for $N \leq 400$ at any activity considered.

We show now, in Fig. 5, that indeed the new model does not change the properties of passive rings in good solvent conditions.
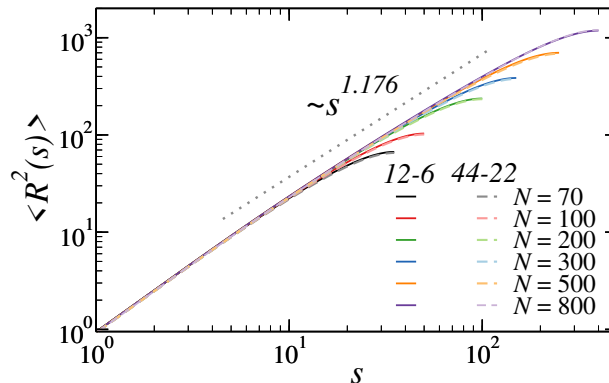

Figure 5. Mean square internal distance as function of the contour separation s for the standard Kremer-Grest model ($12 - 6$ in the legend) and the model employed in this study ($44 - 22$ in the legend) for passive rings of different length in equilibrium.

As visible, the mean square internal distance (defined in the following Section) shows negligible differences, indicating that the conformational properties are the same for both models, as expected. Caution shall be used, though, when employing this model in dense suspensions as the monomers are effectively slightly smaller.

As final remark we notice that, given the choice of employing tangent vectors of fixed length, the total active force, acting on the centre of mass, is not zero: the sum of the tangent vectors is zero by definition, but the corresponding unit vectors do not add up to a perfect zero. This does not affect neither the inflation, the collapse or the arrest, but affects the dynamics of the centre of mass, which may be relevant when considering suspensions of active rings at finite density.

OBSERVABLES

We define here the observables considered in this work: the gyration radius of a polymer of length N is defined as

$$R_g^2 = \frac{1}{N} \sum_{i=1}^{N} (\mathbf{r}_i - \mathbf{r}_{com})^2 \tag{4}$$

where $\mathbf{r}_{com}$ is the position of the center of mass of the polymer; the average value reported in this work has been average over time (at steady state) as well as over a number $250 < M < 2850$ independent realisations.

The root mean square internal distance is defined as

$$\langle R(s) \rangle = \sqrt{\langle (\mathbf{r}_{s+s_0} - \mathbf{r}_{s_0})^2 \rangle} \tag{5}$$

where s is the distance (in beads) along the backbone. The average is performed as above and in addition over the starting bead s_0.

The bond-bond correlation function is defined as

$$\beta(s) = \langle \mathbf{b}_{s+s_0} \cdot \mathbf{b}_{s_0} \rangle \tag{6}$$

where $\mathbf{b}_i = \mathbf{r}_{i+1} - \mathbf{r}_i$ (averages are performed as above).

The tangleness $T(t)$ will be defined as

$$T(t) = \left\langle \frac{(j - j_1)^2 + \ldots + (j - j_m)^2}{m} \right\rangle \tag{7}$$

where j is the index of the beads along the contour, j_i stand for the indices of the spatial neighbours of bead j (first neighbours along the contour are excluded) and the average is performed over all the beads as well as over several realizations.The distance along the contour accounts for the ring topology (i.e. we consider the minimal distance along the contour).

The torsional order parameter is defined following [69] as $U_T = \sum_{i=0}^{N} \cos(\gamma_i)$ where

$$\cos(\gamma_i) = \frac{(\mathbf{b}_{i-1} \times \mathbf{b}_i) \cdot (\mathbf{b}_i \times \mathbf{b}_{i+1})}{|\mathbf{b}_{i-1} \times \mathbf{b}_i||\mathbf{b}_i \times \mathbf{b}_{i+1}|} \tag{8}$$

where $\mathbf{b}_{i-1}$, $\mathbf{b}_i$ and $\mathbf{b}_{i+1}$ are three subsequent bond vectors; the periodicity of the ring is taken into account.

The self-intermediate scattering function is defined as

$$F_s(k^*, t) = \langle \left(\sum_{i}^{N} e^{i\mathbf{k}^* \cdot (\mathbf{r}_i(t) - \mathbf{r}_i(t_0))} \right) \rangle \tag{9}$$

where k^* is a fixed value and $\mathbf{k}^*$ is any vector in reciprocal space of magnitude k^*.

Finally, a standard way to measure the "characteristic" time of a ring in equilibrium is to compute the time correlation function of the vectors normal to the surface of the ring

$$\mathbf{c} = \mathbf{a} \times \mathbf{b} \tag{10}$$

where $\mathbf{a} \equiv \mathbf{r}_{i+N/2} - \mathbf{r}_i$ and $\mathbf{b} \equiv \mathbf{r}_{i+3N/4} - \mathbf{r}_{i+N/4}$; alternatively the time correlation of the vector $\mathbf{a}$ (the "half-ring" vector) may also be considered.

CLUSTERING ALGORITHM AND NEIGHBOUR SEARCH

We describe here how we identify neighbours and how we define the collapsed section of the ring by means of a clustering algorithm. We always consider configurations at steady state. Concerning the permanence of the neighbours, we perform a standard neighbour search, based on their euclidean distance; we consider as neighbours particles within a certain cut-off radius r_c. As mentioned in the main text, we exclude first neighbours along the backbone.

Further, we employ a clustering algorithm to identify the collapsed section in Fig. (4) of the main text. We perform first a neighbour search; we consider all the monomers who are interacting with at least 4 monomers, i.e. whose distance from at least 4 monomers is less than $r_c = 1.2\sigma$, as belonging to a cluster. Joining the clusters defines the collapsed section. The rest of the monomers belong to the dangling sections.

UNKNOTTEDNESS

The study reported in this paper concerns unknotted ring polymers. In order to assess the role of the topology on the conformational and (especially) on the dynamical properties, one has to ensure that the topology is preserved, i.e. the rings must remain unknotted at all times. We tested the unknottedness of the rings using Kymoknot[70]; no knot have been found by means of this test. Further, we check the distributions of the bond length, visible in Fig. 6

We check rings of length $N = 70$ and $N = 500$; we notice that the distributions are very similar at fixed Pe for both cases (the former inflated, the latter collapsed). Further, we notice that the maximum extension of the bonds is 1-2 % of the characteristic bond length $b = 0.96 \ \sigma$ and it is sufficient to prevent crossings.

GHOST RINGS

We consider, in this section, the conformational properties of ghost (or phantom) rings, i.e. rings where non-nearest neighbours along the backbone do not interact with each other. For such rings, topology is not preserved; we check the effect of the activity in such case, in order to highlight the role of topology preservation and steric interactions over the phenomenology observed in the main text (see Fig. 7).

The gyration radius (panel (a)) scales now as $N^{0.5}$ for all the systems considered; activity only swells the rings. This behaviour is different from what observed for gaussian linear chains, that also showed a progressive decrease of the exponent of the gyration radius, at the values of Pe considered here[13]. Notice that the exponent is the right
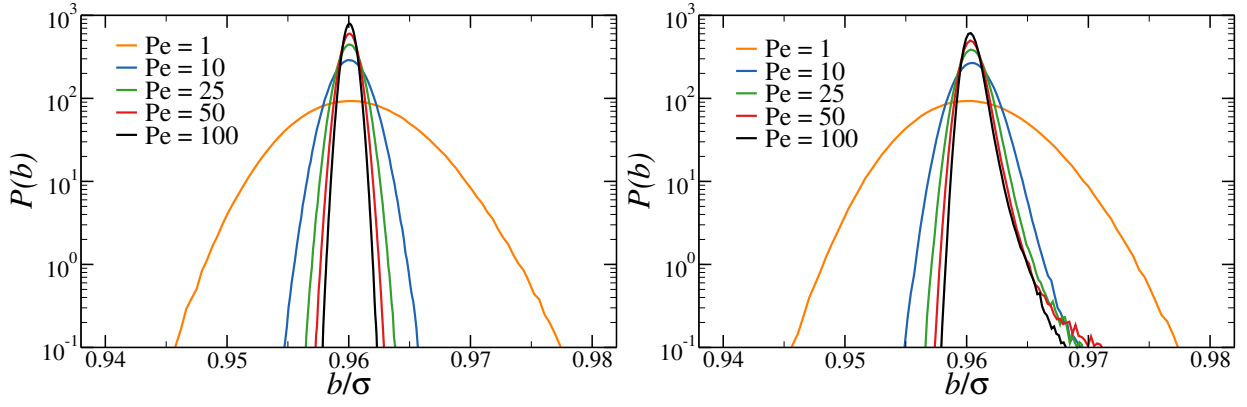
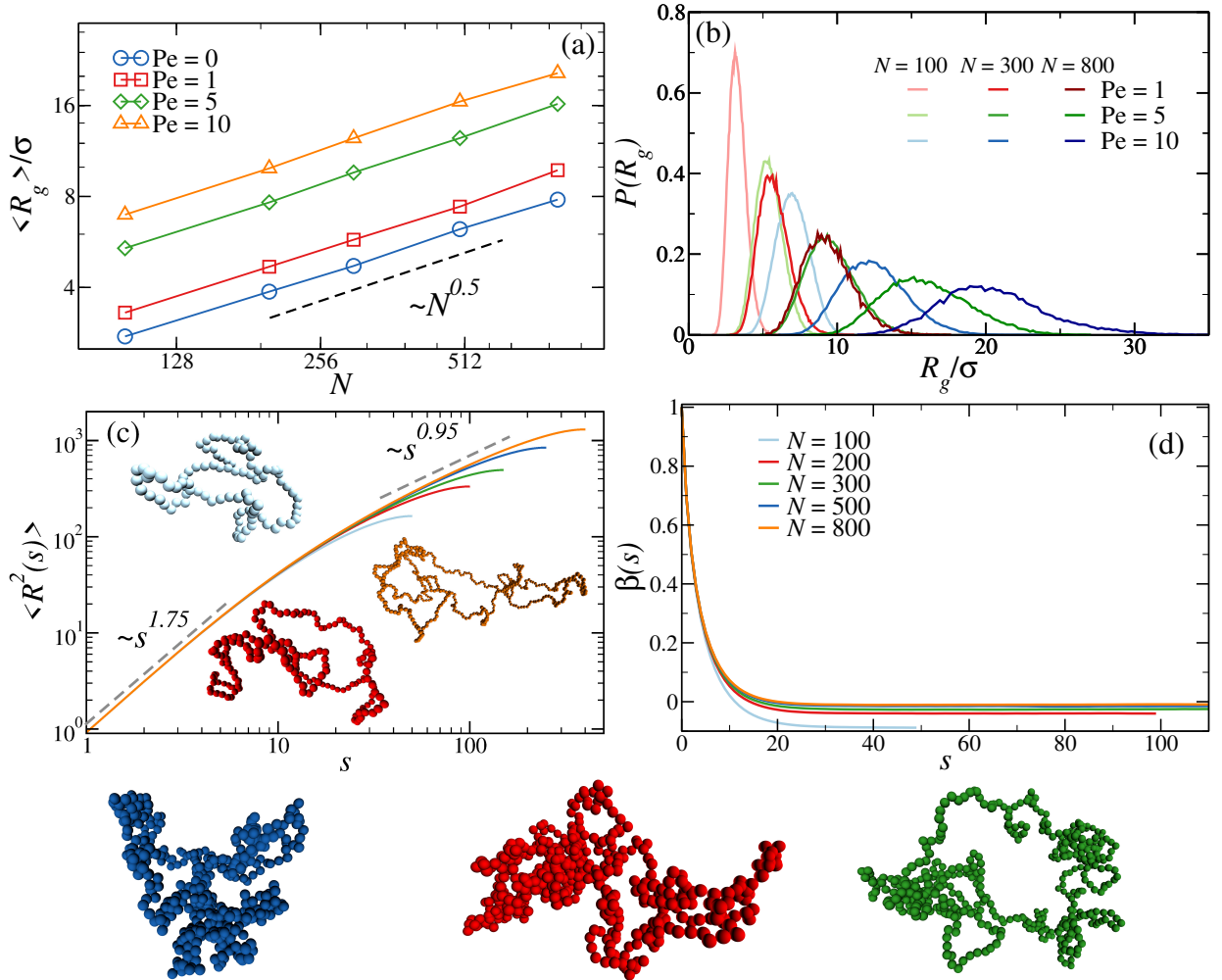Figure 6. Distribution of the bond length of active rings for A) $N = 70$, B) $N = 500$, and several values of Pe.

Figure 7. Configurational properties of ghost rings: A) Gyration radius as function of the ring length N; B) Distributions of the gyration radius; C) Mean square internal distance as function of the contour distance s; D) Bond-bond correlation as function of the contour distance. Snapshots: panel c) light blue $N = 100$, red $N = 200$, orange $N = 500$, all at Pe = 10; bottom row blue Pe = 0, red Pe = 1, green Pe = 5, all of length $N = 500$.

one in the passive case ($\nu = 0.5$), because topology is not conserved. Indeed this is confirmed in panel (b) and (c); notice that the fluctuations of R_g become stronger as we increase Pe. Further, in panel (d) the bond-bond correlation
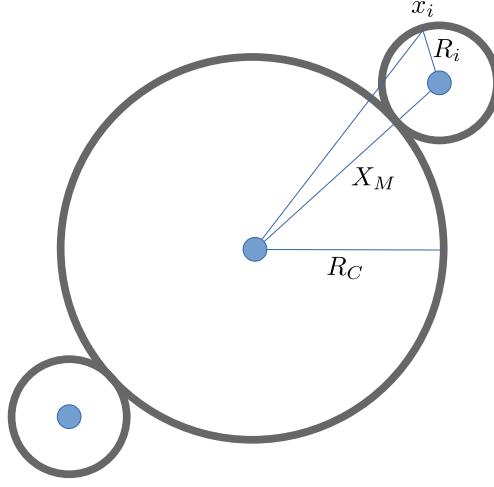
Figure 8. cartoon of a spherical collapsed structure with two equal dangling regions.

does not show the presence of any minimum, indicating that the bonds do not have a preferred organization, with a characteristic size (see snapshots). All these quantities support the observation that, without self-avoidance and topology preservation, formation of tangles is not possible. With respect to gaussian linear chains, buckling happens also there, but cyclisation reduces the space of possible configurations to a subset where buckling does not lead to a size reduction.

THEORETICAL ANALYSIS OF THE SCALING OF R_g WITH N SHOWN IN FIG.1

We derive a simple argument to understand the scaling exponent of the gyration radius R_g with N shown in Fig. 1. In order to get analytical insight we split the monomers into two sets: those that belong to the compact collapsed main structure and those that belong to the dangling sections. We further assume that the $\mathcal{N}$ dangling sections are all composed by M monomers and that their size M is independent on N. The idea behind the latter assumptions is that in the scaling regime i.e., for very long polymers, the size of the dangling sections is determined by some "microscopic" parameters rather then by the polymer length N. Moreover we approximate both the collapsed structure and the dangling regions with spheres of radii R_C and R_M. The gyration radius is defined as

$$R_G^2 = \sum_{i=1}^{N} (x_i - x_{\mathrm{CM}})^2 \tag{11}$$

where x_{CM} is the position of the center of mass that, in practice, coincides with the center of mass of the collapsed structure. The last expression can be rewritten as

$$R_G^2 = \sum_{i=1}^{N-\mathcal{N}M} (x_i - x_{\mathrm{CM}})^2 + \sum_{i=N-\mathcal{N}M+1}^{N} (x_i - x_{\mathrm{CM}})^2 \tag{12}$$

$$= b^2 (N - \mathcal{N}M)^{\frac{2}{3}} + \mathcal{N} \sum_{i=1}^{M} \left(\sqrt{x_M^2 + R_i^2 - 2\cos\alpha_i x_M R_i} - x_{\mathrm{CM}} \right)^2 \tag{13}$$

where the first term on the r.h.s. accounts for the contribution from the monomer is the collapsed structure and the latter from all monomers belonging to the $\mathcal{N}$ identical dangling sections. In particular, in the latter term we have decomposed the distance from the center of mass into the distance to the center of mass of the dangling region plus the distance from it (see Fig. 8).

Without loss of generality we shift the reference frame such that $x_{\mathrm{CM}} = 0$. Moreover we approximate the second term in Eq. (13) as

$$\sum_{i=1}^{M} x_M^2 + R_i^2 - 2\cos\alpha_i x_M R_i \simeq M(x_M^2 + R_M^2) \tag{14}$$

where we have assumed that all the monomers belonging to any single dangling sections are a at distance $\sim R_M$ from its center of mass and that the term proportional to the cosine becomes negligibly small, once we sum over all the monomers. Next, as shown in Fig. 8, we have that

$$x_M = R_C + R_M = b\left(N - \mathcal{N}M\right)^{\frac{1}{3}} + R_M \tag{15}$$

Accordingly, when the number of monomers involved in the dangling sections is small ($\mathcal{N}M \ll N$) Eq. (14) can be approximated by

$$M(x_M^2 + R_M^2) = M(R_C^2 + 2R_c R_M + R_C^2) \simeq MR_C^2 \simeq Mb^2\left(N - \mathcal{N}M\right)^{\frac{2}{3}} \tag{16}$$

Accordingly, the expression for the gyration radius can be be approximated by

$$R_G^2 \simeq b^2\left(N - \mathcal{N}M\right)^{\frac{2}{3}}\left(\mathcal{N}M + 1\right) \simeq b^2 N^{\frac{2}{3}}\mathcal{N}M . \tag{17}$$

where have used that $1 \ll \mathcal{N}M \ll N$. We note that Eq. (17) is indeed function of $\mathcal{M} = \mathcal{N}M$ that is the total number of monomers in the dangling regions. Predicting the scaling of $\mathcal{M}$ with N is a formidable task. Indeed, due to the active nature of the system, we cannot define a free energy and hence we cannot compare any free energy cost with thermal energy as usual in scaling models of passive polymers at equilibrium [71]. Accordingly, we compare Eq. (17) with the outcome of the numerical simulations

$$b^2 N^{\frac{2}{3}}\mathcal{M} \simeq b_\infty^2 N^{2\nu_{\text{long}}} \tag{18}$$

where $b_\infty \approx 0.39 - 0.40$ is a prefactor with dimension of a length that can be extracted from Fig. 1. From the last expression we obtain the scaling of $\mathcal{M}$

$$\mathcal{M} \simeq \frac{b_\infty^2}{b^2} N^{2\nu_{\text{long}} - \frac{2}{3}} . \tag{19}$$

Upon substituting $\nu_{\text{long}} \simeq 0.41$ in Eq. (19) we obtain

$$\mathcal{M} \simeq \frac{b_\infty^2}{b^2} N^{0.15} \tag{20}$$

therefore we expect $\mathcal{M}$ to grow very slowly with N.

NON-EQUILIBRIUM ROUTE TO STEADY STATE

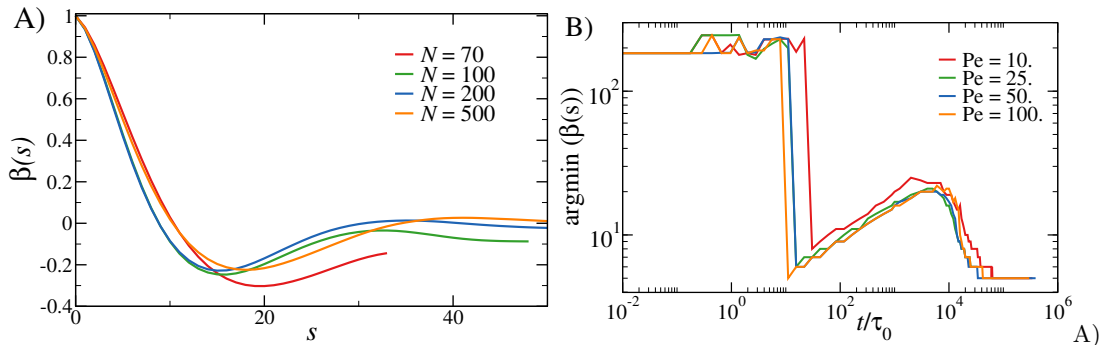We report here more information about the non-equilibrium route to the steady state. We report, in Fig. 9a,

Figure 9. A) Bond-bond correlation as function of the contour distance s for rings of different length, fixed activity Pe $= 100$, measured at the (arbitrary) fixed time $t/\tau_0 = 1300$. B) Position of the minimum of the bond correlation as a function of time, normalized by τ_0, for rings of length $N = 500$ and different values of Pe.

examples of bond-bond correlation functions during the non-equilibrium route to the steady state, taken at the (common) time $t/\tau_0 = 1300$, where τ_0 is the typical diffusion time of a single monomer. An average over $400 < M <$

2850 independent configurations has been carried out. We notice that, as suggested by Fig. 2 of the main text, the position of the minimum is roughly the same for all the values of N considered. Moreover, we consider, in Fig. 9b, the minimum of $\beta(s)$ for fixed length $N = 500$ and various Pe > 10. We observe that the curves display the same features as the curves reported in the main text. In particular, the intermediate growth of $\beta(s)$ is almost independent on Pe (one can observe a slight difference between the curve for Pe $= 10$ and the other curves), while the growth exponent remains the same. We also note that, upon reaching the steady state, the minimum of $\beta(s)$ is independent on Pe, for sufficiently high values of Pe.

Route to steady state at low Pe
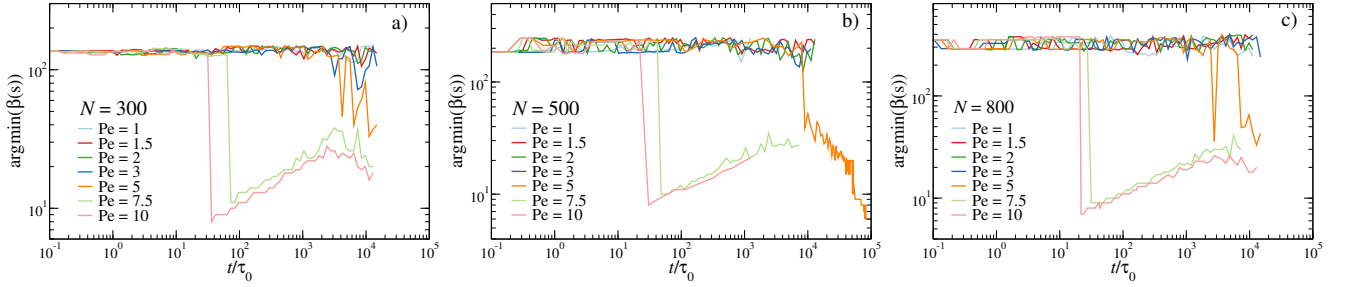
Figure 10. Loci of the minima of the bond-bond correlation argmin$\beta(s)$ as function of time for several Pe ≤ 10 and a) $N = 300$, b) $N = 500$, c) $N = 800$.

In order to better characterize the low-Pe regime, we performed short simulations specifically at $1<$ Pe < 10 and $N \geq 300$. As reported in Fig. 10, we observe that the sudden drop observed at larger Pe disappears. Instead, we observe a less abrupt decrease or no decrease at all (within the investigated time window). Thus, it appears there is an additional pathway at low Pe, where rings still end up in a collapsed state but that does follow the pathway described in the main text. Overall, the fact that the characteristic bends do not develop at low Pe is consistent with a previous result on active linear chains[13], where similar "bends" were really marked only at sufficiently high Pe.
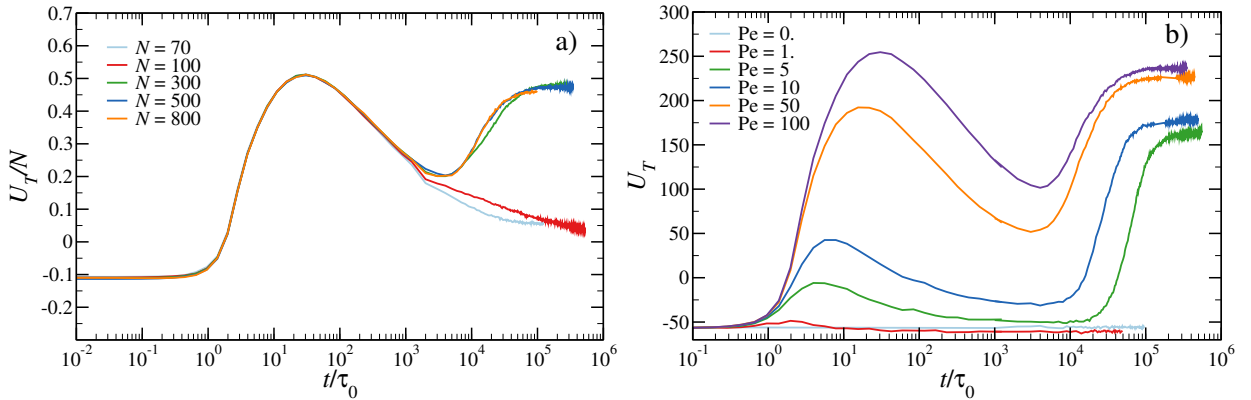
Torsional order parameter

Figure 11. Torsional order parameter U_T as function of time for A) fixed Pe $= 100$, several N; B) fixed $N = 500$, several values of Pe.

In order to characterize further the organization in the collapsed state and, possibly, the pathway to the steady state, we compute the torsional order parameter, defined in Eq. (8) in Section "Observables" and we report it in Fig. 11. The quantity U_T increases as the polymer (or parts of it) assumes an helical conformation and can be used to characterise the helical buckling of polymers in strong flow, where the backbone reacts to a compression/extension in

the direction of the channel's main axis[69]. This compression/extension happens, to some extent, also in tangentially active polymers. Indeed, in Fig. 11, we report U_T as function of time, from a passive, equilibrated conformation to the steady state. We observe that, for all rings, U_T is proportional to N; it also assumes a negative value for passive rings, which is constant in equilibrium (see Fig. 11b), compatibly with the results reported in [69] in the same conditions. For active rings, U_T shows a strong increase within the time window $\tau_0 < t \lesssim 100\tau_0$; the magnitude of the peak as well as its position in time grow larger upon increasing Pe. After the peak, at $t/t_0 \approx 10^4$, U_T continues to decrease for short rings, while it increases again for long rings until it finally reaches a plateau; as visible in Fig. 11b, the value of this plateau depends non-trivially on Pe. Notice that the position in time of this minimum for $N > 300$ is strikingly compatible with the timescale at which we observe the onset of the final collapse in Fig. 2 of the main text. Indeed, the emergence of helical-like structures is perfectly compatible with the anti-correlation observed in the bond correlation function. Further, notice that the fact that U_T/N assumes a large value at the steady state for long rings brings forward a more qualitative description of the organization in the collapsed state, as a structure formed by an internal "core", wrapped all around by other chain segments.

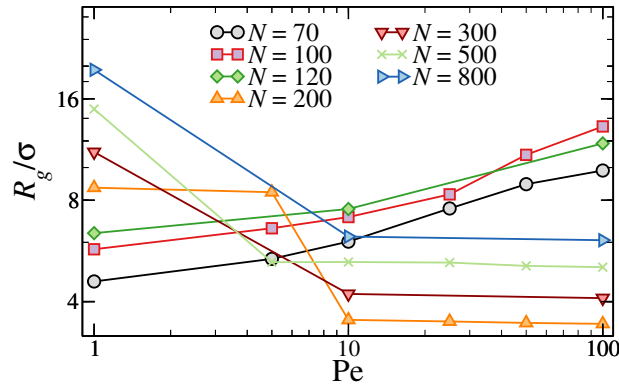## RING CONFIGURATIONAL PROPERTIES AT STEADY STATE

Gyration radius

Figure 12. Gyration radius of as self-propelled ring as function of Pe.

We report, in Fig. 12, the average gyration radius of self-propelled ring polymer as function of Pe. We notice that for short chains, up to $N = 120$, R_g increases upon increasing Pe. Above $N \approx 300$, $\langle R_g \rangle$ become insensitive of Pe, for all Pe > 1 investigated.
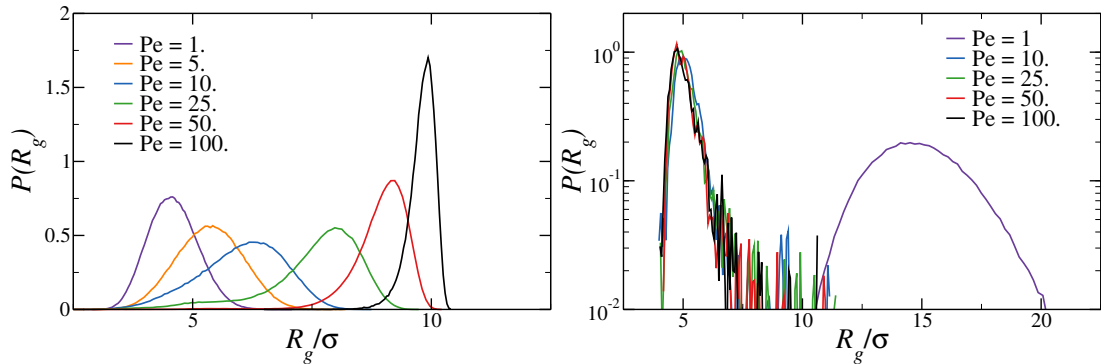

Figure 13. Distribution of the gyration radius of self-propelled rings for $N = 70$ (left panel), B) $N = 500$, (right panel), and several values of Pe.

We further inspect the distributions of the gyration radius, for different values of N and Pe in Fig. 13. Fixing $N = 70$, we notice that the mode of the distribution increases, upon increasing Pe; the distributions become progressively
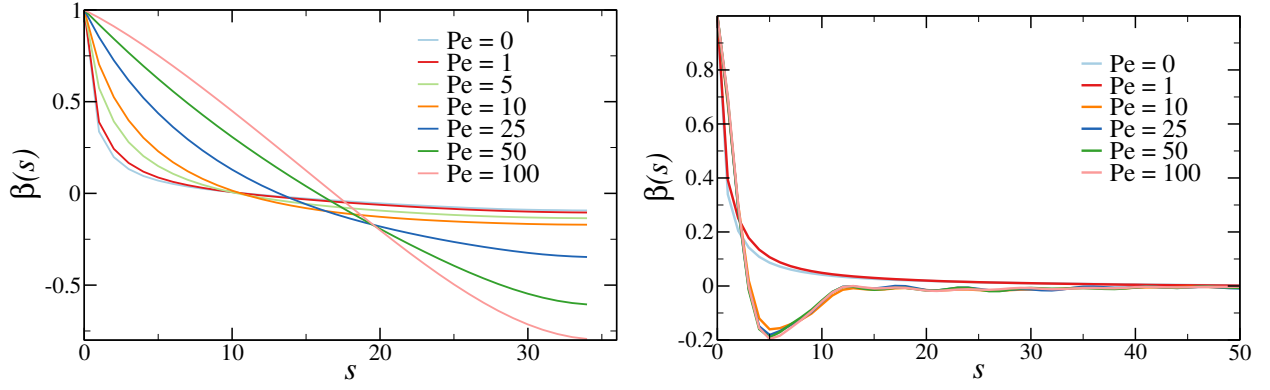
Figure 14. Bond-bond correlation as function of the contour distance s; fixed $N = 70$ (left panel), fixed $N = 500$ (right panel) and several values of Pe.

narrower, i.e. fluctuations are suppressed. For $N = 500$, distributions overlap for Pe > 1.

Bond correlation function

We report here further examples of bond-bond correlations along the contour of the ring, (see Fig. 14).

We focus here on the effect of increasing Pe for rings of different sizes $N = 70$ (short) and $N = 500$ (long). Notice that the function, for short rings, shows a progressively marked minimum at $s = N/2$ upon increasing Pe, akin of progressively more rigid rings. On the contrary, for long rings the functions at Pe > 1 completely overlap and show a common minimum at $s \simeq 5$. This hints at the fact that, aside of having typical "spires" or "wraps" of 5 beads, the collapsed section is randomly organized; notice, though, that this fact also supports the universality of the route to collapse we described in the main text.
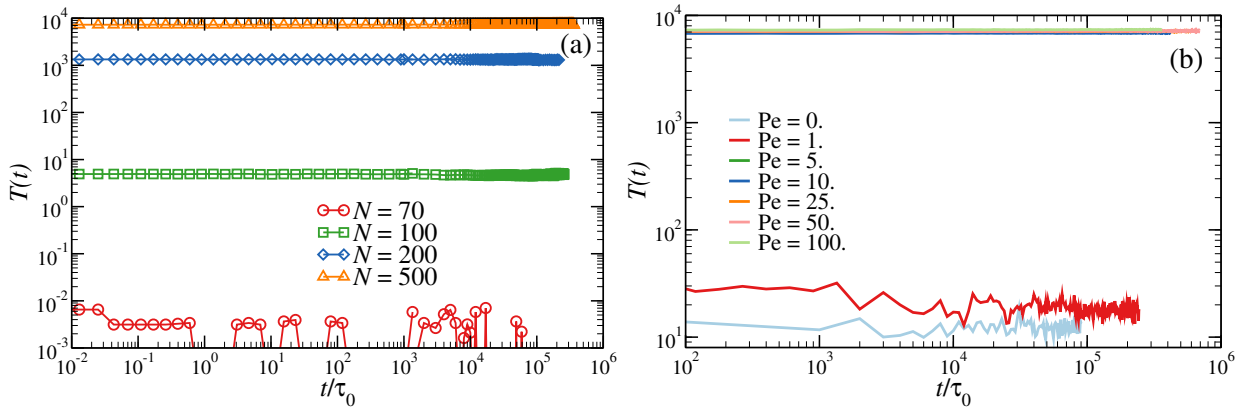
Tangleness

Figure 15. Tangleness $T(t)$, defined in Eq. (7), as a function of time in the steady state for (a) rings of different length N at fixed Pe = 100, (b) rings of fixed $N = 500$ and different values of Pe.

In Fig. 15, we show $T(t)$ as function of time during the steady state. As for $\mathrm{argmin}(\beta(s))$, also $T(t)$ remains constant, the particular value attained is characteristic of the ring length and increases upon increasing N (see panel a). Such increase, given the definition of $T(t)$, is reasonable in a collapsed state as, increasing N, larger contour distances between monomers may be achieved. Further, the tangleness greatly increases upon increasing Pe at fixed N (panel b): clearly, this massive difference reflect the fact that the system is in a collapsed state for sufficiently high values of Pe.

COLLAPSED RINGS INTERNAL DYNAMICS AT THE STEADY STATE

Neighbour survival

We report here further data regarding the neighbour survival $S(t)$, i.e. the the average fraction of original neighbours as function of time.
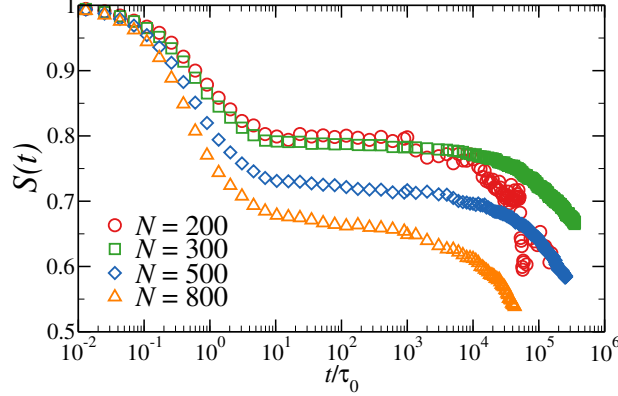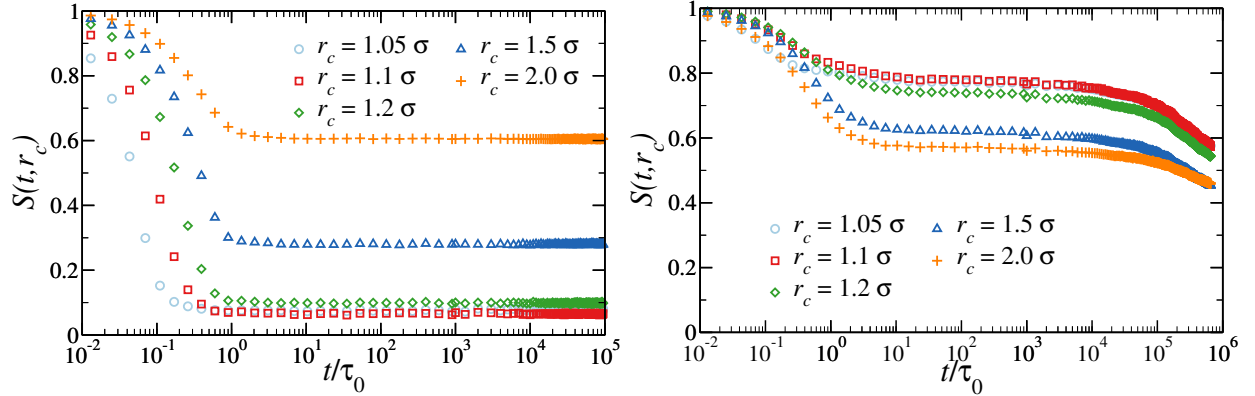

Figure 16. Fraction of survived neighbours as function of time for rings of length $N = 500$ and Pe $= 0$ (left panel), Pe $= 25$ (right panel).

In Fig. 16, we report $S(t)$ for rings of different length. We can appreciate how the length of the plateau in time does not change for $200 < N < 500$ and only slightly diminishes for $N = 800$.

In the main text, the cut-off value chosen for this quantity is $r_c = 1.2~\sigma$, which is a bit larger than the potential cut-off value 1.032σ. We check the effect of the cut-off radius r_c on $S(t)$ in Fig. 17. As we employ this observable

Figure 17. Fraction of survived neighbours as function of time for rings of length $N = 500$ and Pe $= 0$ (left panel), Pe $= 25$ (right panel) and different values fo the cut-off radius r_c, used in the definition of the neighbour search.

to characterize the collapsed state, we focus to a specific length $N = 500$ and on a specific activity Pe $= 25$; we also report the passive case Pe $= 0$. In both cases, we find that the shape of the curve remains the same for all r_c investigated. We notice that, for the passive rings (left panel), the value of the final plateau grows upon growing r_c as beads progressively further along the backbone are identified as neighbours and remain permanently close by. On the contrary, in the collapsed case the value of intermediate plateau diminishes. Choosing a large cut-off radius in the collapsed state implies to select more neighbours, for any given monomer. This means that increasingly more monomers have neighbours belonging to the rather mobile dangling sections; small rearrangements influence more monomers. Thus quantitatively the overall permanence diminishes but, qualitatively, the plateau remains.

Self-intermediate scattering function

We report here the self-intermediate scattering functions $F_s(k)$ for active rings; $F_s(k)$ is usually employed to characterize the dynamics of arrested states, as it reveals the characteristic time scales of the system.
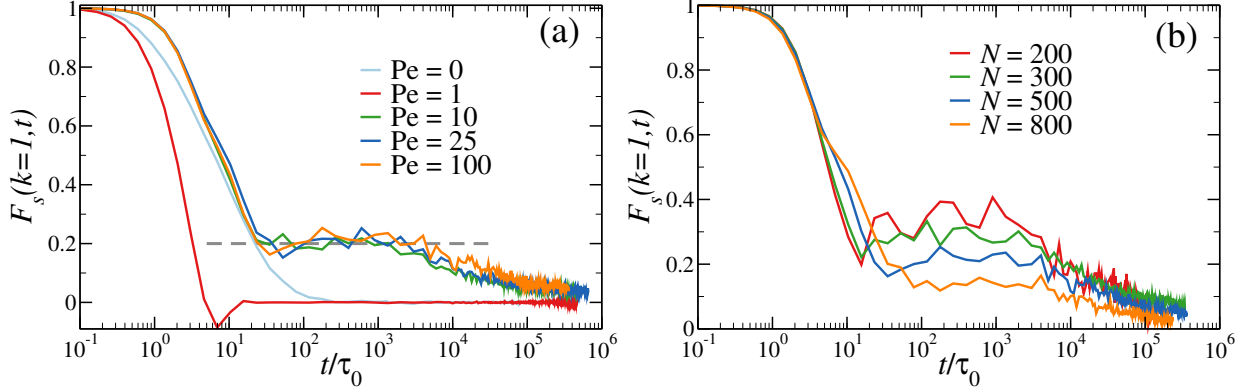

Figure 18. Self intermediate scattering function for (a) fixed $N = 500$ and different values of Pe and (b) fixed Pe $= 100$ and several values of N.

We report, in Fig. 18 the intermediate scattering function for either rings of fixed length $N = 500$ (panel a) or fixed activity Pe $= 100$(panel b). In panel (a), $F_s(k)$ for the non-collapsed cases Pe $= 0$, 1 shows a single decay; interestingly, for Pe $= 1$ it also shows a negative dip, observed in self-propelled systems[72]. When rings collapse (Pe > 1 for $N = 500$), $F_s(k)$ shows a double decay, a well known hallmark of arrested systems.

In Fig. 18b, we compare the self-intermediate scattering function for rings of different length at fixed Pe (all cases considered feature collapsed configurations in the steady state). Observe that the double decay is present for all N considered and, in this case, the length of the plateau is independent on N.

When calculating the self-intermediate scattering function, one usually chooses to fix the magnitude of the wave vector k as the value at which the maximum of the static structure factor occurs. As the form factor of a macromolecule does not show, usually, any well defined peak, we show here the effect of using k-vectors of different magnitude (see Fig. 19).
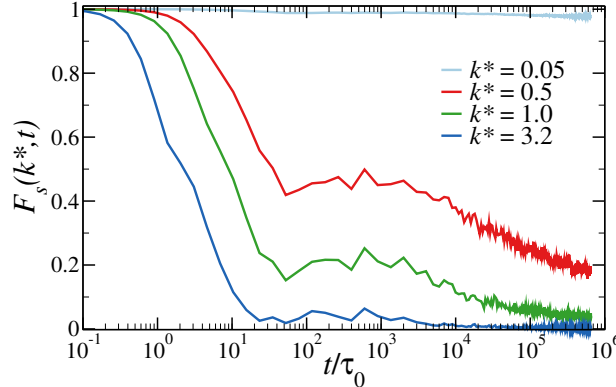

Figure 19. Self intermediate scattering function for rings of fixed $N = 500$ and Pe $= 25$ and different values of k.

We focus on collapsed rings ($N = 500$, Pe $= 25$ in Fig. 19). We observe that, if k is very small, the relaxation time probed is the one of the overall macromolecule; it is thus extremely long and not fully developed during the time of the simulation. On the other hand, for $k > 1$ the dynamics probed concerns length scales smaller than the monomer size σ and we thus observe only a fast relaxation. Otherwise, for $k \approx 1$ we observe the presence of a two step relaxation process, as reported in the main text.

Ring time correlation functions

The last two quantities we investigate in order to characterise the arrest of the collapsed rings are two time correlation functions: the correlation of the "half-ring" vector, i.e. the vector connecting any monomer with its furthest peer $N/2$ far away along the contour, and the correlation of the vector normal to the surface of the ring, defined in Section "Observables".
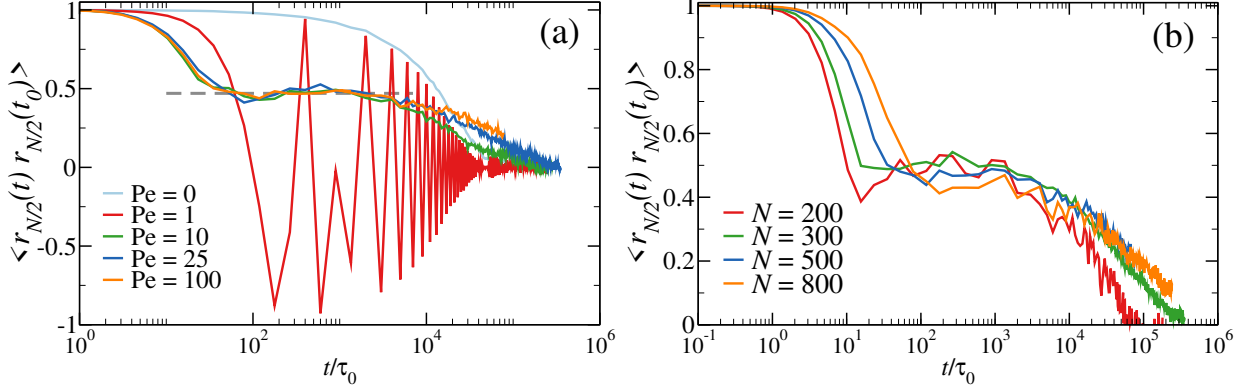

Figure 20. Time correlation of the half-ring vector for rings of fixed length $N = 500$ and different Pe $= 0$ (panel a), fixed Pe $= 100$ and different N (panel b).

We report, in Fig.20 the time correlation of the "half-ring" vector $r_{N/2}$. For the passive case, the function exhibits a single decay. For Pe $= 1$, we observe an oscillatory behaviour, fairly regular, whose intensity decays over time, following the decay of the passive ring. This behaviour reveals an overall rotation of the ring, fairly regular, powered by the activity. A single rotation happens, roughly, over $10^2\tau_0$. In the case of the collapsed rings, interestingly we notice again the presence of a double decay; in Fig. 20b, we notice it is present for all N investigated.

Further, we report in Fig. 21 the correlation time of the vector normal to the surface of the ring, defined in Eq. (10).
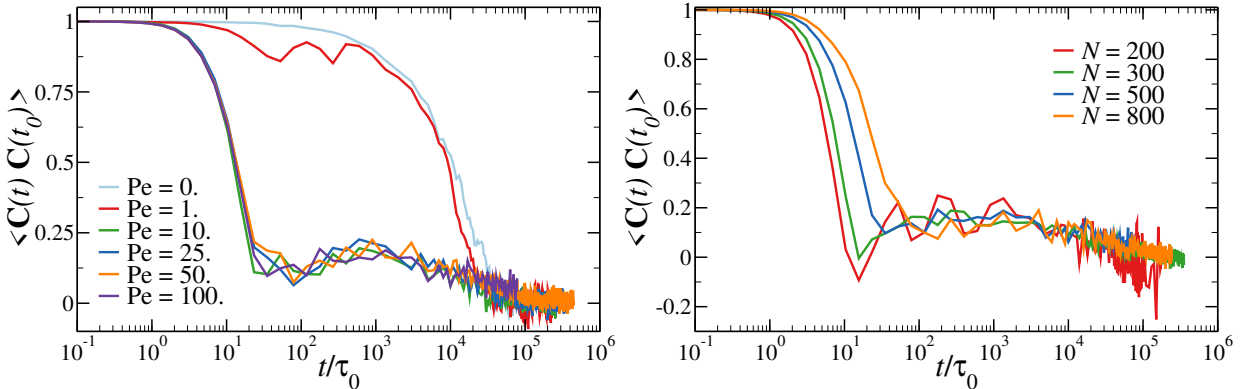

Figure 21. Time correlation of the characteristic vector (see Eq. (10)) for ring of fixed $N = 500$ and several values of Pe (panel a) and fixed Pe $= 100$ and different N (panel b).

In Figure 21a, we again notice that Pe $= 0,1$, cases that do not feature any collapse, are quite similar among each other. Indeed the effect of the activity, for Pe $= 1$, is simply to rotate the ring and, for this particular observable, does not induce any drastic change. For all the other values of Pe investigated, we again observe a double decay, as well as, in Fig. 21b, for all the different values of N reported (which, again, all collapse).

For these time correlations, the double decay indicates the presence of fast-evolving sections, which we ascribe to the sections outside of the collapsed part of the ring (dangling sections in the main text) and of very slow regions (or possibly a single region) that freeze the evolution of the dynamics for a period of time and further impede the relaxation of the whole ring at very long times.

Velocity distributions

We show here the distribution of the monomer velocities for rings of different lengths (see Fig. 22, left panel).
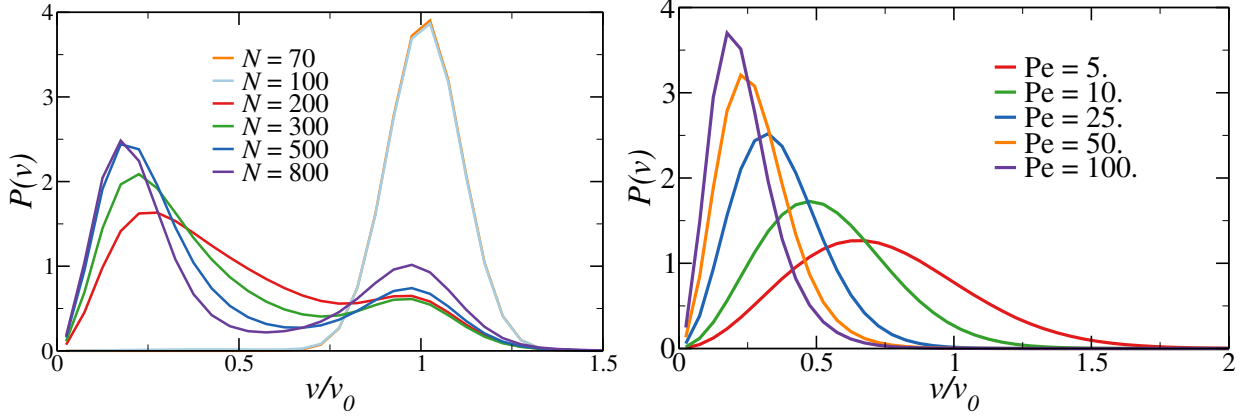

Figure 22. (right panel) Monomer velocity distributions for rings of fixed Pe $= 100$ and several values of N. (Left panel): Monomer velocity distributions at the steady state for fixed $N = 500$, several Pe; distributions are limited to monomers belonging to the collapsed section.

For rings that are not collapsed, the distribution is peaked around $v = v_0$, i.e. the mean velocity of the active monomers; for collapsed rings, we observe for all N the presence of two peaks, as described in the main text. Interestingly, both the first and the second peak grow increasing N; this suggests that, for longer rings, dangling sections are more common than for shorter rings and, in general, monomer segregate into very slow or very mobile groups. Finally, in right panel of Fig. 22 we observe the distribution of the velocity of individual monomers for the same systems reported in the main text (Fig. 4a); here we consider, using the cluster algorithm described in the Section "Clustering Algorithm and Neighbour Search", only the monomers belonging to the collapsed sections. Indeed, we confirm that the slow monomers are the ones belonging to the collapsed sections; by exclusion, fast monomers belong to the dangling sections.
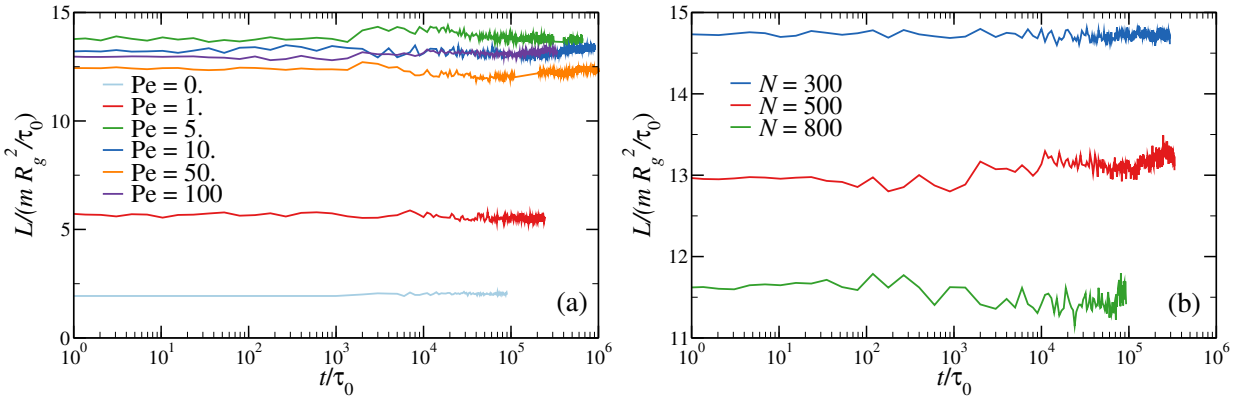
Angular velocity at the steady state for large rings

Figure 23. Average of the angular momentum magnitude over the average size of the ring $L/(m\,R_g^2/\tau_0)$ as function of time for a) fixed $N = 500$, several values of Pe; b) fixed Pe $= 100$, several N.

We compute the angular momentum in the frame of reference of the centre of mass

$$\mathbf{L} = \sum_{i=1}^{N} \mathbf{r}_i \times \mathbf{p}_i\,, \tag{21}$$

where $\mathbf{r}_i$ and $\mathbf{p}_i$ are the distance from the center of mass and the linear momentum of the monomer i, respectively. We report, in Fig. 23, the average magnitude of the angular momentum $L = \langle |\mathbf{L}| \rangle$, normalized by by $m\,R_g^2/\tau_0$. Such quantity provides an estimation of the state of angular velocity of the object, as the angular momentum is normalized by the average size of the ring. In Fig. 23a, we compare $L/(m\,R_g^2/\tau_0)$ for rings of fixed length $N = 500$ and different values of Pe. We observe that the average angular momentum magnitude is constant in time and its value is larger for Pe > 5, in comparison with Pe = 0,1 cases: notice that all rings at Pe > 5 are collapsed. In Fig. 23b) we compare $L/(m\,R_g^2/\tau_0)$ for rings with a fixed value of Pe = 100 and three values of $N = 300, 500, 800$; here all three cases display collapsed conformations at the steady state for the chosen value of Pe. We observe that smaller rings have a larger rotational motion; possibly, they are powered by a proportionally larger active torque as the collapsed section is less disordered than for larger rings. The results suggest that, indeed, collapsed rings possess a higher rotational motion with respect to non-collapsed rings of the same size.